Chemico-Biological Interactions 418 (2025) 111563

Contents lists available at ScienceDirect

Chemico-Biological Interactions

journal homepage: www.elsevier.com/locate/chembioint

Research paper

Comprehensive transcriptomic analysis in wild-type and ATM knockout lung cancer cells: Influence of cisplatin on oxidative stress-induced senescence

Ayşegül Varol [a], Sabine M. Klauck [b], Susan P. Lees-Miller [c], Thomas Efferth [a,*]

[a] Department of Pharmaceutical Biology, Institute of Pharmaceutical and Biomedical Sciences, Johannes Gutenberg University-Mainz, 55128, Mainz, Germany
[b] Division of Cancer Genome Research, German Cancer Research Center (DKFZ) Heidelberg, National Center for Tumor Diseases (NCT), NCT Heidelberg, a partnership between DKFZ and University Hospital Heidelberg, 69120, Heidelberg, Germany
[c] Department of Biochemistry and Molecular Biology, Robson DNA Science Centre, Charbonneau Cancer Institute, Cumming School of Medicine, University of Calgary, 3330 Hospital Drive NW, Calgary, AB, T2N 1N4, Canada

ARTICLE INFO

Keywords:
Chemotherapy resistance
Personalized cancer therapy
Prognostic biomarkers signal transduction
Survival analysis
Transcriptomics

ABSTRACT

Genetic mutations and impaired DNA repair mechanisms in cancer not only facilitate tumor progression but also reduce the effectiveness of chemotherapeutic agents, particularly cisplatin. Combination therapy has emerged as a promising strategy to overcome resistance. Comprehensive transcriptomic analyses, supported by integrated comparative bioinformatics and experimental approaches, are essential for identifying biomarkers and novel therapeutic targets underlying drug resistance. In this study, we performed overall survival and mutation analyses, examining 23 double-strand break repair proteins across more than 7500 tumors spanning 23 distinct cancer types. Our findings identify ATM (ataxia-telangiectasia mutated) as a key protein with the highest mutation frequency.

Using CRISPR/Cas9, we investigated the effects of ATM mutations on signalling pathways that influence the cellular response to cisplatin. ATM knockout enhanced cisplatin cytotoxicity by activating alternative cell death pathways, including oxidative stress-induced senescence and necroptosis. Microarray analysis revealed a regulatory interplay between ATM and NRF2 in the activation of oxidative stress-induced senescence. Specifically, ATM knockout promoted senescence by increasing reactive oxygen species (ROS) accumulation and down-regulating NRF2 expression.

To enhance combination therapy, integrating genetic profiling with advanced tools such as CRISPR/Cas9 to target oxidative stress-induced senescence may provide innovative strategies to overcome drug resistance, thereby advancing personalized cancer treatment. These approaches lay the foundation for the development of personalized cancer therapies tailored to the unique mutational landscape of individual patients, offering promising prospects for improving treatment outcomes.

1. Introduction

DNA damage is an inevitable consequence of cellular metabolism, resulting from both endogenous factors such as reactive oxygen species (ROS) and exogenous factors such as ultraviolet (UV) radiation [1–3]. This damage can manifest in single-strand breaks (SSBs) and double-strand breaks (DSBs), which are among the most detrimental forms of DNA lesions [4,5]. To maintain genomic stability and preserve cellular function, mammalian cells employ a complex DNA damage response (DDR), which halts the cell cycle and initiates repair mechanisms to restore the integrity of the genome [5,6]. However, if these repair mechanisms fail or are overwhelmed, mutations can accumulate,

Abbreviations: ATM, Ataxia-telangiectasia mutated; cDNA, Complementary DNA; DRM, DNA repair mechanism; DDR, DNA damage response; DSB, Double-strand breaks; H_2DCFH-DA, 2′7-Dichlorodihydrofluorescein diacetate; IPA, Ingenuity Pathway Analysis; NRF2, Nuclear factor (erythroid-derived 2)-like 2; PI, Propidium iodide; PBS, Phosphate-buffered saline; PS, Phosphatidyl serine; ROS, Reactive oxygen species; SA-β-gal, Senescence-associated β-galactosidase; SSB, Single-strand breaks; TCGA, The Cancer Genome Atlas; UV, Ultraviolet radiation.

* Corresponding author.
E-mail address: efferth@uni-mainz.de (T. Efferth).

https://doi.org/10.1016/j.cbi.2025.111563
Received 28 February 2025; Received in revised form 30 April 2025; Accepted 15 May 2025
Available online 16 May 2025

leading to cellular dysfunction and contributing to the development of age-related diseases and cancer [7]. Cancer progression is driven by the accumulation of genetic mutations, as well as the impairment of key defence systems, including DNA repair mechanisms and cellular death pathways [8]. While the individual impact of these mutations may be minimal, their cumulative effects can significantly alter cellular function, making them crucial drivers of cancer initiation and progression [8]. Moreover, the presence of mutations leads to resistance to cancer therapies, particularly chemotherapeutic agents [9].

Cisplatin resistance is one of the most common challenges encountered in cancer chemotherapy [10]. Cisplatin induces cell cycle arrest and apoptosis by binding to DNA and forming crosslinks [11,12]. However, its effectiveness is often limited by drug resistance, which can result from mutations in drug target sites or changes in related cellular pathways [13]. Especially, acquired mutations in DNA repair and cell death genes can reduce cisplatin sensitivity, prompting the exploration of combination therapy as a strategy to overcome resistance. Successful combination therapy requires identifying biomarkers to develop drugs that bypass resistance mechanisms and improve treatment outcomes.

An integrated approach that combines biomarker expression profiling with genetic polymorphism analysis is crucial for accurately assessing a patient's drug resistance status. The impact of specific biomarkers can vary depending on tumor type, stage, metastasis, and patient-specific factors such as age, gender, and genetic background. To avoid the identification of conflicting or unreliable biomarkers, a comprehensive bioinformatic analysis is necessary. In this regard, we conducted a thorough investigation into the mutations and survival data of 23 proteins involved in the double-strand break DNA repair (DSB) mechanism across 23 distinct cancer types. Using theedistinct parameters, we identified mutation hotspots in protein-coding regions, with particular focus on missense, nonsense, and frameshift mutations. Our analysis revealed ATM (ataxia-telangiectasia mutated) as a key protein with the highest mutation frequency, particularly missense mutations, which varied across different cancer types. Notably, these mutations were observed in a subset of lung cancer patient samples, positioning ATM as a potentialcandidate for a predictive biomarker in lung cancer.

Additionally, we explored the effect of 23 distinct DNA repair proteins on survival across multiple cancer types by encompassing more than 7500 patient samples. We found that several biomarkers with high expression levels were associated with poor survival outcomes, particularly in lung, kidney, breast, and liver cancers. These findings highlight the need for personalized therapeutic approaches that take into account the unique mutational and expression profiles of individual patients.

The advent of CRISPR/Cas9 gene-editing technology has garnered significant attention in the scientific community for its potential to manipulate the genome in cancer cells [14]. The CRISPR/Cas9 platform provides a powerful tool to investigate the functional roles of specific genes or mutations in the context of cancer development [15–17]. By utilizing CRISPR/Cas9-based ATM knockout lung cancer cells, we assessed how targeting ATM influences cisplatin sensitivity. In the presence of ATM, cell death pathways, particularly apoptosis and autophagy, are activated in response to cisplatin exposure. However, the activation of cell death pathways was observed at higher doses of cisplatin. This suggests that existing mutations in ATM could restrict the proper response of these signalling pathways, leading to reduced sensitivity to cisplatin.

In contrast, the knockout of ATM through combination therapy has activated alternative cell death pathways. In particular, oxidative stress-induced senescence and necroptosis have been identified as key mechanisms responsible for the increased cisplatin sensitivity observed by ATM knockout. Oxidative stress, which results from an imbalance between the production of reactive oxygen species (ROS) and the antioxidant defence system, can trigger senescence, a stable arrest of the cell cycle that plays an important role in tumor suppression. Focusing on the genes or pathways that drive oxidative stress-induced cellular senescence could provide new opportunities for inhibiting cancer progression and overcoming drug resistance [18].

In our study, we performed microarray hybridization and bioinformatic analyses to uncover the interaction between ATM and nuclear factor (erythroid-derived 2)-like 2 (NRF2), a key regulator of the antioxidant response. Our findings are consistent with the existing knowledge in the literature [19,20]. Additionally, it demonstrates that senescence induced by oxidative damage is regulated through NRF2 and ATM signalling pathways. The suppression of NRF2, either directly or indirectly, significantly promoted cellular senescence, highlighting its potential as a therapeutic target for overcoming cisplatin resistance [21].

Thus, understanding the complex interplay between DNA repair, cell death pathways, and drug resistance mechanisms is essential for developing more effective cancer therapies. The integration of novel technologies such as CRISPR/Cas9 with biomarker profiling offers exciting prospects for personalized medicine, contributing ultimately to improve outcomes for those with cancer.

2. Material and methods

2.1. Determination of mutational hotspot sites

We determined the mutational hotspot sites in 23 genes involved in DSB. The UniProt database and cBioPortal, an open-access platform for exploring cancer genomics data, open the opportunity to detect the domains for each gene [22,23]. The sequence data of more than 7500 tumor patients were classified into three categories: missense mutations, nonsense mutations, and frameshift mutations.

Initially, data were downloaded from the open-access databases on the cBioPortal website (https://www.cbioportal.org/) by entering 23 different cancer studies and gene names. Subsequently, a more in-depth analysis was performed separately for each of the 23 genes. Rather than focusing on the total number of mutations found for each gene, the analysis specifically identified the number of missense, nonsense, and frameshift mutations in the domain regions. After determining the total number of mutations in the different domain regions, each gene was compared, and regions with a high density of mutations were identified. Supplementary Table S1 presents a representative example of the mutation analysis of the ATM gene obtained via the cBioportal platform. Our focus directed to those genes with the highest mutational hotspots, and *ATM* has been selected.

2.2. Overall survival analysis

To assess the survival probability of cancer patients associated with the mRNA expression of 23 DSB genes, we utilized the Cancer Genome Atlas (TCGA) dataset obtained from cBioportal (https://www.cbioportal.org; accessed between 2020 and 2021) as our primary data source. The TCGA dataset provided comprehensive information on 23 different cancer types, encompassing the expression levels of 23 distinct DSB genes, as well as five pathoclinical key parameters: age, race, gender, metastasis, and tumor stage. Combining multiple existing cohorts into a single, unified dataset can significantly support the identification and validation of reliable prognostic biomarkers [24]. For this purpose, we have performed survival analyses using the Kaplan-Meier (KM) plotter, a platform for performing survival analysis using transcriptomic data of large patient cohorts.

At the outset of the analysis, separate Excel files were generated for each parameter using data obtained from cBioPortal. Within these files, patient outcomes were encoded as "1" for surviving patients and "0" for deceased patients. Regarding the age parameter, each of the seven age groups (10–20, 20–30, 30–40, 40–50, 50–60, 60–70, 70–80) was analyzed separately. Subsequently, we conducted Kaplan-Meier survival analyses for each DSB gene (as stated in a previous [25]), utilizing the SPSS program (IBM Corp. Released 2015. IBM SPSS Statistics for Windows, Version 23.0. Armonk, NY: IBM Corp).

Table 1
Selected primer for qPCR experiment.

Gene Symbol	Forward Primer	Reverse Primer
GAPDH	TTCGACAGTCAGCCGCATCT	CCGACCTTCACCTTCCCCAT
CDKN2A	CTGCCCAACGCACCGAATAG	CCACCAGCGTGTCCAGGAAG
IL8	CTTTCCACCCCAAATTTATCAAAG	CAGACAGAGCTCTCTTCCATCAGA
IL6	CCGGGAACGAAAGAGAAGCT	GCGCTTGTGGAGAAGGAGTT

To determine the statistical significance, we employed the "log-rank" test statistics. By applying this statistical test, we identified survival curves that exhibited noteworthy differences. Specifically, we considered survival curves with a *p*-value below 0.05 as statistically significant. We selected the cancer types most affected by genes responsible for poor patient survival.

2.3. Knockout of ATM using CRISPR/nCas9-mediated genome editing

Gene knockout of ATM was conducted as previously described (performed by Dr. Yaping Yu at the Center for Genome Engineering, Cumming School of Medicine, University of Calgary) [26]. The CRISPR-Cas9 system was employed to delete ATM using the pSpCas9 (BB)-2A-GFP (pX458) plasmid, incorporating a short guide RNA sequence targeting exon 9 of ATM (5′-TACGTTCCCCATGTCGCTGT-3′). All short guide oligonucleotides were synthesized, annealed, and inserted into the pX458 plasmid, with successful cloning verified through DNA sequencing at the University of Calgary's DNA laboratory.

Forty-eight hours following transfection of A549 CRISPR-ATM cells, the cells were collected, and genomic DNA was extracted utilizing the KAPA Express Extract Kit (Kapa Biosystems) in accordance with the manufacturer's guidelines. PCR was performed to amplify genomic DNA fragments of ATM surrounding the short guide RNA target site.

2.4. Cytotoxicity assay

To detect the cytotoxicity of anticancer drugs, we used the resazurin reduction assay, which measures the cellular metabolic activity rather than direct cytotoxicity and is influenced by stress responses such as senescence or growth arrest, which may not involve immediate apoptosis or necrosis [27,28]. Specifically, the impact of cisplatin, carboplatin, and 5-fluorouracil was investigated over a concentration range of 0.003–100 μM, targeting both $ATM^{+/+}$ A549 and $ATM^{-/-}$ A549 cancer cell lines. To execute the experiments, the cells were seeded into 96-well plates, and upon reaching 70 %–80 % confluence, they were treated with the drugs for 72 h. Subsequently, the cells were incubated for 4 h with 20 μL resazurin (Sigma-Aldrich, Taufkirchen, Germany) per well, diluted in double-distilled water (ddH_2O). The fluorescence was detected using an excitation wavelength of 544 nm and an emission wavelength of 590 nm with the Infinite M2000 Pro™ plate reader (Tecan, Crailsheim, Germany). IC_{50} values were calculated using nonlinear regression analysis in Microsoft Excel.

2.5. Microarray-based expression profiling for predicting canonical pathways

To investigate the transcriptomic landscape of *ATM*-driven gene regulation in A549 cells, we performed microarray hybridization expression analyses. Both $ATM^{+/+}$ and $ATM^{-/-}$ A549 cells were exposed to IC_{50} concentrations of cisplatin (9.91 μM and 3.36 μM, respectively) for 24 h. After treatment, total RNA was extracted using the InviTrap® Spin Universal RNA Mini Kit from Invitek Molecular (Berlin, Germany). The extracted RNA was then converted to complementary DNA (cDNA), labeled, and hybridized onto Affymetrix GeneChips® using the human ClariomS™ assay (Affymetrix, Santa Clara, CA, USA) at the Genomics and Proteomics Core Facility of the German Cancer Research Center (DKFZ, Heidelberg, Germany). The gene expression was analyzed with Chipster software (version 3.16.3, https://chipster.csc.fi/) (accessed on June 21, 2020), focusing on differential expression and statistical significance determined by the empirical Bayes *t*-test ($p < 0.05$).

Chipster software is an open-source software used for bioinformatics analyses. Specifically, Chipster can be employed for the comparison of data derived from different databases. For instance, it can be used for differential expression analysis to compare gene expression levels. In our study, we initially prepared data from $ATM^{+/+}$ and $ATM^{-/-}$ A549 cells without cisplatin treatment using the Chipster software and visualized the results through the IPA (Ingenuity Pathway Analysis) software from Ingenuity Systems (Redwood City, CA, USA, content version 51963813, released on July 31, 2023) (Fig. 4). Subsequently, we compared the data from cisplatin-treated $ATM^{+/+}$ A549 cells with that of wild-type A549 cells not exposed to any treatment using the Chipster software and uploaded IPA software to visualized (corresponding to the $ATM^{+/+}$ A549 data shown in Fig. 5). The same analysis was also applied to compare cisplatin-treated $ATM^{-/-}$ A549 cells with untreated counterparts (corresponding to the $ATM^{-/-}$ A549 data shown in Fig. 5). We compared the impact of cisplatin on these cell lines by generating gene expression-based heatmaps and analyzed canonical signalling pathways using activation z-scores and p-values as key metrics.

2.6. Quantitative real-time q-PCR for validating relative gene expression

After performing transcriptomic analyses, our objective was to validate the microarray hybridization findings through q-PCR analysis. For this purpose, we designed primers using the Primer BLAST online tool (https://www.ncbi.nlm.nih.gov/nucleotide/, accessed in 2023) and obtained them from Eurofins Genomics (Ebersberg, Germany). The specific primers selected for the study are listed in Table 1. The expression of *GAPDH* was selected as an internal control.

Subsequently, we treated $ATM^{+/+}$ and $ATM^{-/-}$ A549 cancer cells with cisplatin concentrations equivalent to their respective IC_{50} values of 9,91 μM and 3,36 μM, respectively, for 24 h. Total RNA extraction was performed using the InviTrap® Spin Universal RNA Mini Kit (Invitek Molecular, Berlin, Germany), followed by mRNA to cDNA conversion using the LunaScript® RT SuperMix Kit cDNA Synthesis Kit (New England Bio Labs, Darmstadt, Germany).

For gene amplification, we utilized the EvaGreen master mix (5 × Hot Start Taq EvaGreen® q-PCR Mix (no ROX); Axon Labortechnik, Kaiserslautern, Germany) following the manufacturer's instructions. Q-PCR was conducted on a CFX384TM instrument (Bio-Rad, Munich, Germany) using a 38-well plate and running 40 cycles. The PCR run conditions included an initial denaturation phase at 95 °C for 15 s, followed by a gradient annealing step ranging from 62 °C to 47 °C for 30 s, and finally, an elongation step at 72 °C for 1 min. To determine the fold-change in gene expression, we employed the comparative Cq (2-ΔΔCq) method [29].

2.7. Cell cycle analysis

Cells were seeded at a density of 3×10^5 cells per well in 6-well plates and treated with distinct cisplatin concentrations (9.91 μM for $ATM^{+/+}$ A549 cells and 3.36 μM for $ATM^{-/-}$ A549 cells) for 24 h. Following treatment, both cell lines were fixed with ethanol and stored at −20 °C for an additional 24 h. Fixed samples were then subjected to centrifugation (4000 rpm, 10 min) and re-suspended in 500 μL of cold

PBS supplemented with 20 μg/mL RNase (Roche Diagnostics, Mannheim, Germany). Then, we used 50 μg/mL propidium iodide (PI) (Sigma-Aldrich, Darmstadt, Germany) for staining. Stained samples were measured using a NovoCyte Quanteon flow cytometer (Agilent) and data analysis was performed using FlowJo software (version 10.8.1) (BD Life Sciences). For each sample, 10,000 cells were recorded. The gating was performed by forward and side scatter properties (FSC–H/SSC-H), and further gating for single cells (PI-YG561nm 615/20-A/PI-YG561nm 615/20-H) in a linear manner was applied to remove doublets or debris. PI staining was detected using a 561 nm laser and 615/20BP filter. Each experimental procedure was independently replicated three times. Data analysis was further completed using GraphPad Prism 6 (La Jolla, CA, USA) software for presentation and interpretation.

2.8. Detection of apoptosis

Apoptotic and necrotic cell populations were assessed and quantified using Annexin V/PI staining, following established protocols [30]. This methodology was recently described in detail in our prior study [31]. Annexin V is a calcium-dependent phospholipid-binding protein that interacts specifically with phosphatidylserine (PS). During the initiation of apoptosis, PS translocates from the inner leaflet of the plasma membrane to the extracellular surface. Propidium iodide (PI), a membrane-impermeable dye, is excluded by viable or early apoptotic cells with intact membranes, but it intercalates with DNA in cells undergoing late apoptosis or necrosis, emitting red fluorescence.

$ATM^{+/+}$ A549 and $ATM^{-/-}$ A549 cancer cells were exposed to varying concentrations of cisplatin (9.91 μM and 3.36 μM, respectively) for 72 h. Subsequently, the cells were stained with Annexin V and PI (BioVersion/Biocat, Heidelberg, Germany) under dark conditions and analyzed using a BD Accuri™ C6 Flow Cytometer. Each experiment was independently conducted in triplicate to ensure reproducibility.

2.9. Detection of reactive oxygen species

We investigated the response of $ATM^{+/+}$ and $ATM^{-/-}$ A549 cancer cells in terms of the generation of reactive oxygen species (ROS). Cells were cultured at a density of 3×10^5 cells per well and exposed them to varying concentrations of cisplatin (9.91 μM for $ATM^{+/+}$ A549 cells and 3.36 μM for $ATM^{-/-}$ A549 cells) for 24 h. Following treatment, cells were collected, washed with PBS, and resuspended in 1 mL PBS. To assess oxidative stress, cells were incubated at 37 °C for 30 min with 10 μM 2′7-dichlorodihydrofluorescein diacetate (H_2DCFH-DA) from Sigma-Aldrich. As a positive control, cells were treated with 50 μM H_2O_2 for 15 min. Live cell staining was performed using 10 μL of DAPI (50 μg/mL). The fluorescence intensity was measured using the median fluorescence intensity of H_2DCFH-DA in a NovoCyte Quanteon flow cytometer (Agilent). The data analysis was performed using FlowJo software (version 10.8.1) (BD Life Sciences). 20,000 cells were recorded for each sample by flow cytometry. Single cells were gated based on forward and side scatter properties (FSC-A/SSC-A), and further gating (FSC-A/FSC-H) in a linear manner was applied to remove doublets or debris. Living cells, indicated by DAPI negative staining, were detected using a 405 nm laser and 445/45BP filter, while H_2DCFH-DA fluorescence was detected using a 488 nm laser and 525/45BP filter. Each experimental condition was independently replicated three times, and data were analyzed using GraphPad Prism 6 software.

2.10. Detection of cellular senescence

To assess cellular senescence in the absence of *ATM*, we employed the senescence-associated β-galactosidase (SA-β-gal) staining protocol using a commercially available kit (Senescence β-Galactosidase Staining Kit, Cell Signalling Technology, Hitchin, Herts, UK Cat no. #9860) [32]. $ATM^{-/-}$ and $ATM^{+/+}$ A549 cancer cell lines were seeded at a density of 3×10^5 cells per well in 6-well plates. After a 24 h incubation, the cell

Table 2
Specific mutational hotspot sites and the mutation frequency therein of 23 DSB-related genes.

Gene	Missense	Nonsense	Frameshift	Mutation Hotspots Domain	Total mutation number
ATM	44	2	3	PI3_PI4_kinase domain (2714–2961)	49
ATR	37	3	3	PI3_PI4_kinase domain (2323–2567)	43
BLM	29	0	3	DEAD/DEAH box helicase (671–838)	32
PRKDC	21	3	1	NUC194 domain (1814–2209)	25
XRCC4	20	0	2	DNA double-strand break repair and V(D)J recombination protein XRCC4 (1–334)	22
XRCC5	15	1	4	Ku70/ku80 β_barrel domain (252–453)	20
XRCC6	14	0	4	Ku70/ku80 N_terminal α/βdomain (37–255)	18
RAD54L	17	0	1	SNF2 family N-terminal domain (156–463)	18
XRCC2	14	1	2	RAD51 (43–205)	17
RAD54B	11	5	1	RAD51 (83–338)	17
RAD51	15	1	1	RAD51 (83–338)	17
RAD50	13	1	2	AAA domain (6–262)	16
WRN	12	2	1	DEAD/DEAH box helicase (551–710)	15
LIG4	11	1	1	DNA ligase N-terminus (14–209)	13
NBN	7	1	2	Nbs1 (683–746)	10
MRE11	7	1	0	MRE11 DNA-binding presumed domain (294–461)	8
DCLR1B	8	0	0	β-Lactamase superfamily domain (23–148)	8
RAD52	6	0	1	RAD52/22 family double-strand break repair protein (35–180)	7
SETMAR	6	0	1	SET domain (150–262)	7
NHEJ1	4	1	0	XLF cernunos, XRCC4-like factor, NHEJ component (11–172)	5
DCLR1A	3	2	0	DNA repair metallo-β-lactamase (914–1019)	5
XRCC3	3	0	2	RAD51 (64–338)	5
APLF	2	1	0	Zinc finger motif (377–402)	3

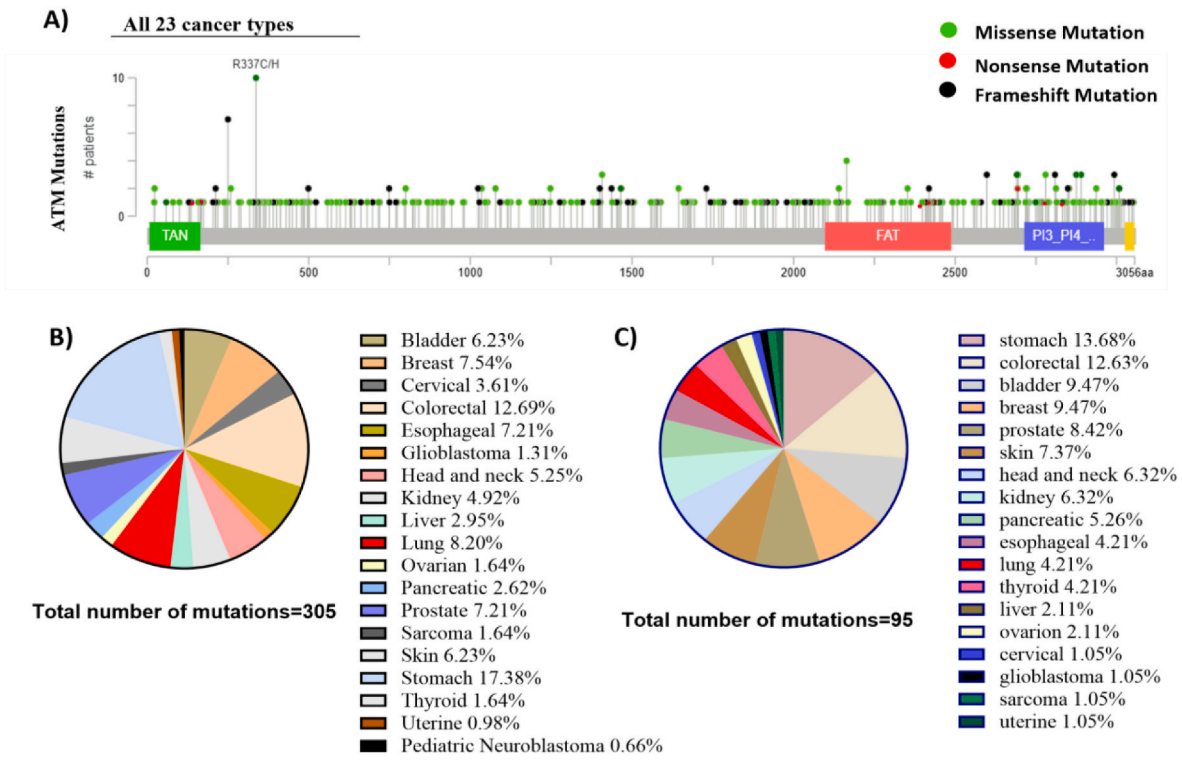

Fig. 1. Gene mutation analysis across 23 different cancer types. (A) The distribution of mutation profiles associated with *ATM. (*B) Percentage distribution of total mutations in the *ATM* gene, including both coding and non-coding regions. (C) Percentage distribution of mutations located exclusively in the coding regions of the *ATM* gene.

lines were exposed to distinct concentrations of cisplatin (9.91 μM for $ATM^{+/+}$ A549 cells and 3.36 μM for $ATM^{-/-}$ A549 cells) for 24 h. Following the treatment, the growth medium was aspirated, and the cells were rinsed twice with 1X phosphate-buffered saline (PBS). Subsequently, cells were fixed by adding 1 mL of 1X Fixative Solution per well and incubated at room temperature for 10–15 min. After fixation, the cells were washed twice with 1X PBS. Next, 1 mL of β-galactosidase staining solution was added to each well, and the plates were incubated at 37 °C overnight in a dry, CO_2-free incubator. Finally, the stained cells were examined under a light microscope equipped with a camera, using a 10 × or higher objective lens. For each of sample, we selected more than 5 images to calculate the percentage of senescent cells. The percentage of SA-β-gal-positive cells (blue staining) was calculated by counting the number of positive cells *versus* the total number of cells, with a minimum of 100 cells counted per condition.

2.11. Single cell electrophoresis (comet assay)

We utilized the comet assay (by using the Oxiselect™ Comet Assay Kit (3-Well Slides) from Cell Biolabs/Biocat (Heidelberg, Germany). $ATM^{+/+}$ A549 cells and $ATM^{-/-}$ A549 cells were initially seeded at a density of 3×10^5 cells per well in 6-well plates. These cells were then treated with cisplatin concentrations corresponding to their respective IC_{50} values (9.91 μM for $ATM^{+/+}$ A549 cell and 3.36 μM for $ATM^{-/-}$ A549 cell 24 h) and H_2O_2 (as a positive control) at a concentration of 50 μM for 15 min.

Following treatment, cells were collected, centrifuged at 3000×*g* for 10 min, and reconstituted in PBS. Cell suspensions at a concentration of 1×10^5 cells/mL were mixed with molten agarose (at a ratio of 1:6) at 37 °C. The resulting mixtures were spread onto comet slides and incubated in darkness at 4 °C for 30 min. Slides were then immersed in a pre-chilled lysis buffer (containing NaCl, EDTA solution, and 10 × lysis solution at pH 10.0) for 1 h at 4 °C. After lysis, slides were transferred to a pre-chilled alkaline electrophoresis solution buffer (containing NaOH, EDTA solution, and distilled water) for 40 min at 4 °C in darkness.

The slides were placed in an electrophoresis chamber filled with the alkaline electrophoresis solution buffer, and electrophoresis was conducted at 20 V for 20 min. After electrophoresis, slides underwent two washes with pre-chilled distilled water for 5 min each. Subsequently, slides were immersed in cold ethanol (70 %) for 5 min and air-dried. Once dried, 100 μL of Vista Green DNA dye (diluted at a ratio of 1:10,000 in TE buffer) was added to each slide and incubated for 15 min at room temperature. Fifty comets from each treatment group were randomly selected and analyzed using OpenComet, a software tool integrated within Image J, developed by the National Institutes of Health. Tail DNA% served as the parameter for quantifying DNA damage [33]. The images obtained showed comets which were captured using a 10 × objective lens, highlighting detailed structural and compositional features.

3. Results

3.1. Determination of mutational hotspot sites

We concentrated on mutations in domain site to detect most predictive biomarker in cancer patients. We determined mutation hotspot sites for 23 genes involved in DSB. Finally, we focused on ATM as the most probable predictive target. As displayed in Table 2, *ATM* contained the highest mutation numbers in comparison of specific mutational hotspot sites of the selected 23 genes involved in DBS. Supplementary Table 1 provides a more detailed representation of the *ATM* mutation analysis derived from the 23 selected cancer cases. Additionally, Fig. 1A visually illustrates the distribution of ATM mutations across the 23 cancer cases. Fig. 1B illustrates the percentage distribution of total mutations observed in both coding and non-coding regions of the *ATM* gene across 23 distinct cancer types. In this study, however, we primarily focused on mutations located within the coding regions. Accordingly, Fig. 1C presents the percentage-based frequency of

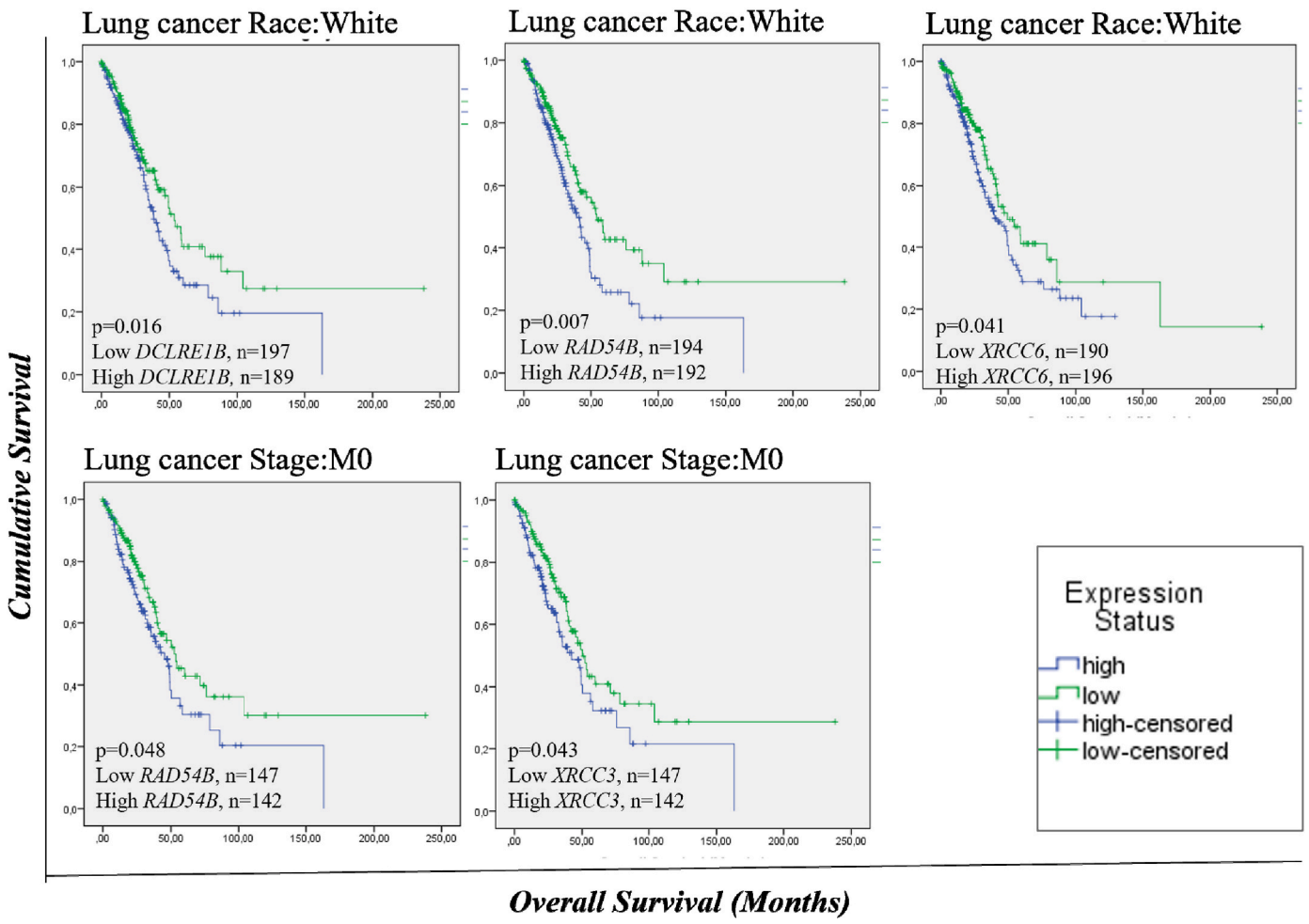

Fig. 2. Biomarkers associated with poor patient survival in lung cancer, as identified through overall survival analysis, are presented ($p < 0.05$)

mutations identified exclusively in the coding regions.

3.2. Overall survival analyses

To identify effective biomarkers, we investigated DSB repair genes with high expression levels associated with poor survival across 23 distinct cancer types. The identified biomarkers are presented in Supplementary Fig. S1. These findings emphasize the substantial biological diversity among cancer types and the context-dependent nature of prognostic biomarkers. Notably, a higher number of prognostic biomarkers were identified in kidney, breast, liver, sarcoma, lung, thyroid, and cervical cancers, suggesting these malignancies may involve more complex and heterogeneous biological mechanisms. Our aim was to focus on one of the cancer types with the highest number of identified prognostic biomarkers, making lung cancer the focal point of this study. Given its clinical significance, lung cancer was selected as the primary focus of this study. The biomarkers identified through survival analysis for lung cancer are presented in Fig. 2.

3.3. Cytotoxicity assay

The cytotoxicity assay was conducted using cisplatin, carboplatin, and 5-fluorouracil. We compared the differences between the $ATM^{+/+}$ A549 and $ATM^{-/-}$ A549 cell lines. Upon treatment for 72 h, the $ATM^{-/-}$ A549 cells exhibited diminished cell viability compared to the wild-type cells in response to the afore-mentioned drugs (cisplatin, carboplatin, and 5-fluorouracil).

Specifically, the $ATM^{-/-}$ A549 cells demonstrated IC_{50} values at a cisplatin concentration of 3.36 ± 1.31 μM, a carboplatin concentration of 14.5 ± 12.55 μM, and a 5-fluorouracil concentration of 0.5 ± 0.08 μM. In comparison, the wild-type cells exhibited IC_{50} values at a cisplatin concentration of 9.91 ± 2.5 μM, a carboplatin concentration of 39.3 ± 4.3 μM, and a 5-fluorouracil concentration of 1.7 ± 0.6 μM (Fig. 3).

3.4. Microarray-based mRNA expression profiling for predicting canonical signalling pathways

For comprehensive transcriptomic analysis of ATM, we performed microarray hybridization-based expression profiling analyses and consecutive Ingenuity Pathway Analysis (IPA). Firstly, to investigate the effects of ATM knockout by using CRISPR/Cas9 technologies, we compared mutant and wild-type A549 cancer cells without cisplatin exposure using IPA analysis (Fig. 4). The absence of ATM impacted signalling pathways involved in cancer cell proliferation, ultimately leading to the suppression of cellular proliferation. It was clearly observed that the NRF2-mediated oxidative stress response, mTOR, EIF2, NOTCH4, and WNT/β-catenin signalling pathways were down-regulated by ATM knockout.

To comprehensively elucidate the mechanisms underlying the enhancement of cisplatin sensitivity through ATM knockout, we conducted a microarray hybridization expression profiling analysis via IPA to compare mutant and wild-type A549 cancer cells under treatment with cisplatin (Fig. 5). The data obtained indicate that, in the presence of ATM, cisplatin response predominantly activated pathways related to autophagy, intrinsic pathway for apoptotic signalling, and MYC-

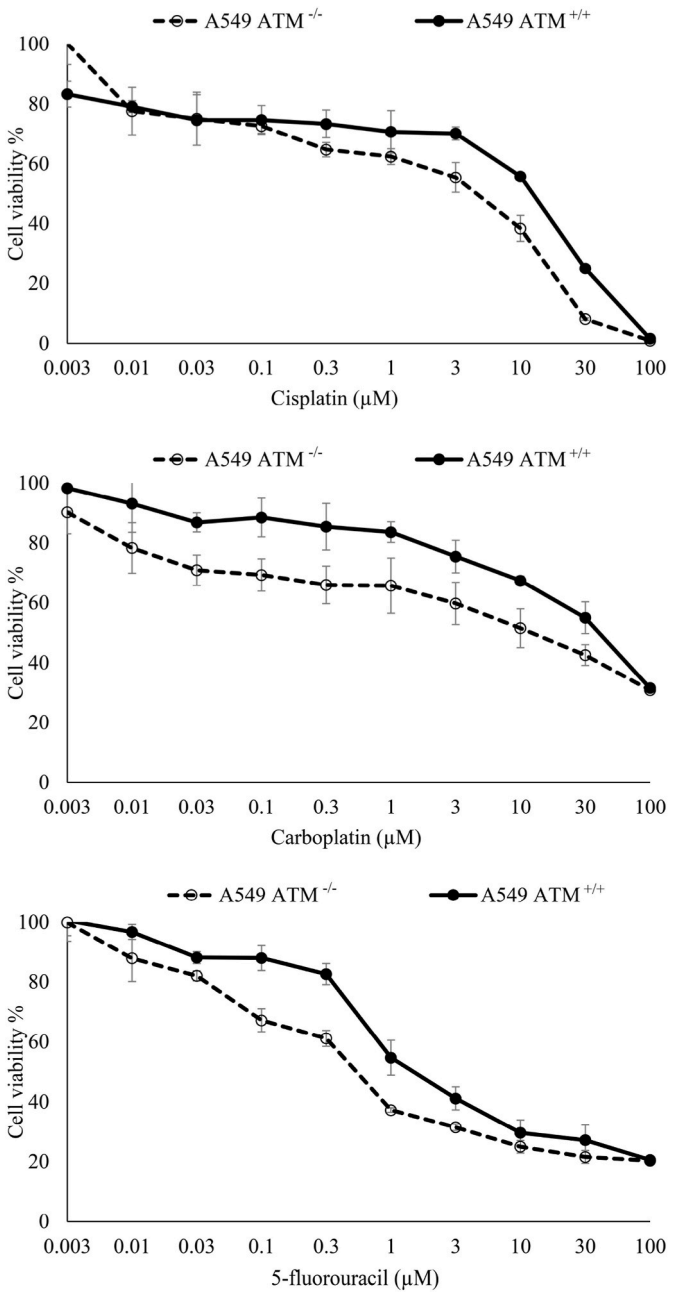

Fig. 3. The cell viability of $ATM^{+/+}$ and $ATM^{-/-}$ A549 cells by using different concentrations of cisplatin, carboplatin, and 5-fluorouracil.

mediated apoptotic signalling. However, in the absence of ATM, the cellular response to the drug shifted, leading to an increased activation of alternative cell death pathways. As illustrated in Fig. 5, despite lower concentrations of cisplatin, the activation of necroptosis, oxidative stress induced senescence and ferroptosis cell death signalling pathways was heightened, while the sub-pathways of autophagy, such as mitophagy and macroautophagy, appear to lose their influence. Especially, oxidative stress-induced senescence promotes cancer cell death, potentially mediated by the downregulation of NRF2. ATM may exert its effects on ROS through its interaction with NRF2, which could influence senescence triggered by oxidative stress.

At this point, mutations present in the ATM gene may render the response to cisplatin more resistant and lead to the activation of cell death signalling pathways only at higher concentrations of cisplatin. In the context of treatment development, employing combination therapies that target distinct cell death pathways through different agents may represent a promising strategy rather than increasing drug dose concentrations.

3.5. Quantitative real-time q-PCR for validating relative gene expression

To validate the microarray hybridization findings, we selected three upregulated and three downregulated genes from both sets including $ATM^{-/-}$ A549 and $ATM^{+/+}$ A549 and performed quantitative PCR (qPCR). The qPCR results were compared with the microarray data, and linear regression analysis along with Pearson correlation coefficients were calculated (Fig. 6A and B). The results were consistent with and supportive of the microarray data. To demonstrate the activation of the oxidative stress induced senescence signalling under ATM knockout, qPCR was performed after cisplatin exposure for two and experimental sets. In the *ATM* knockout A549 cancer cells following cisplatin exposure, the results revealed an upregulation in the expression of *CDKN2A, IL8*, and *IL6,* which play active roles in the oxidative stress-induced senescence signalling pathway (Fig. 6C). Particularly, IL8 and IL6 are two well-characterized factors involved in senescence [34,35].

3.6. Cell cycle analysis

ATM is an important part of cell cycle machinery. Thus, possible mutations in *ATM* result in a change of the cell cycle process upon specific cellular stimuli. Especially, the altered cellular responses after drug treatment by existing mutations may open opportunities for cancer cells to resist the detrimental effects of anticancer drugs. In the absence of functional ATM, cisplatin-induced S-phase arrest decreased, but G2/M arrest considerably increased even at low cisplatin concentrations (Fig. 7).

3.7. Apoptosis

To investigate the effect of ATM knockout on apoptosis, we performed an Annexin-V apoptosis assay. Following cisplatin exposure, an increase in necrosis was observed under ATM knockout, whereas apoptosis was more pronounced in wild-type cells (Fig. 8).

After cisplatin exposure, the percentage of necrotic (dead) cells increased from 50.8 % to 60.3 % in $ATM^{-/-}$ A549 cells, whereas in $ATM^{+/+}$ A549 cells, the percentage of necrotic (dead) cells rose from 6.11 % to 19.6 %. In $ATM^{-/-}$ A549 cells, apoptotic cells slightly decreased from 2.44 % to 0.94%. In contrast, in $ATM^{+/+}$ A549 cells, apoptotic cells increased from 0.46 % to 5.84 %. These values represent the average of three repetitions conducted at different times.

3.8. Detection of reactive oxygen species

We investigated the relation between *ATM* knockout and ROS by different cisplatin concentrations. We measured increased ROS levels depending on *ATM* knockout despite the exposure to only low concentration of cisplatin (Fig. 9). By employing the microarray hybridization technology, gene expression patterns were scrutinized to unravel the intricate interplay between *ATM* knockout and the cellular defence mechanisms against ROS. Our findings suggest that *ATM* knockout disrupted the intricate network of genes involved in ROS defence, thereby compromising the cell's ability to combat oxidative stress.

3.9. Detection of cellular senescence

To determine the effect of *ATM* knockout on cellular senescence, we performed β-galactosidase (β-Gal) staining. Despite exposure to lower concentrations of cisplatin under *ATM* knockout, cellular senescence was enhanced (Fig. 10). The percentage of cells exhibiting senescence was higher under *ATM* knockout.

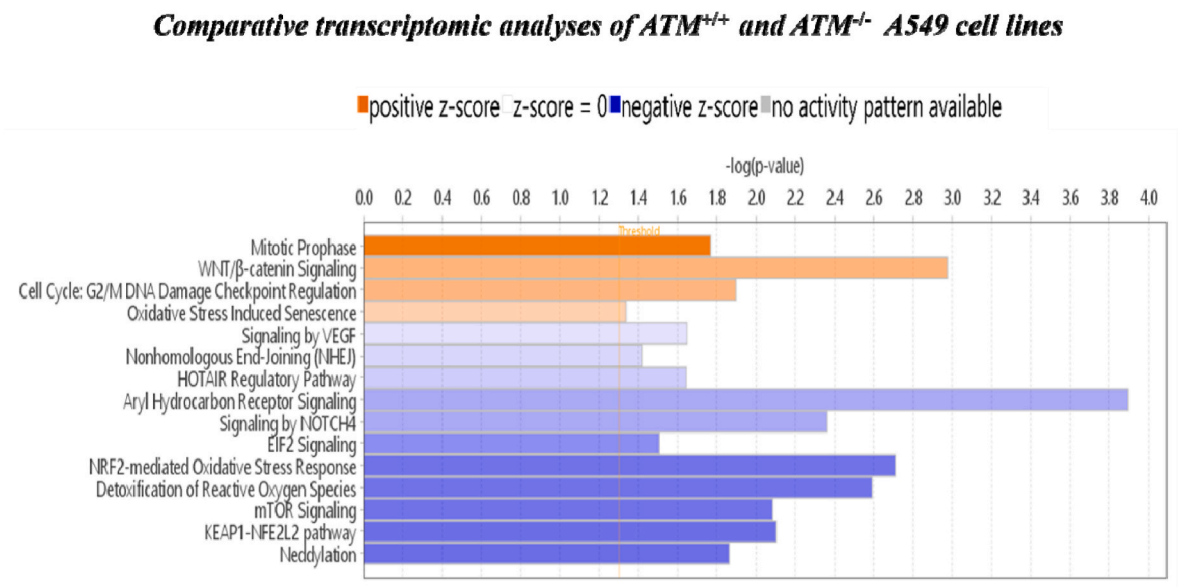

Fig. 4. Canonical pathway analysis of $ATM^{-/-}$ and $ATM^{+/+}$ A549 cells without cisplatin exposure.

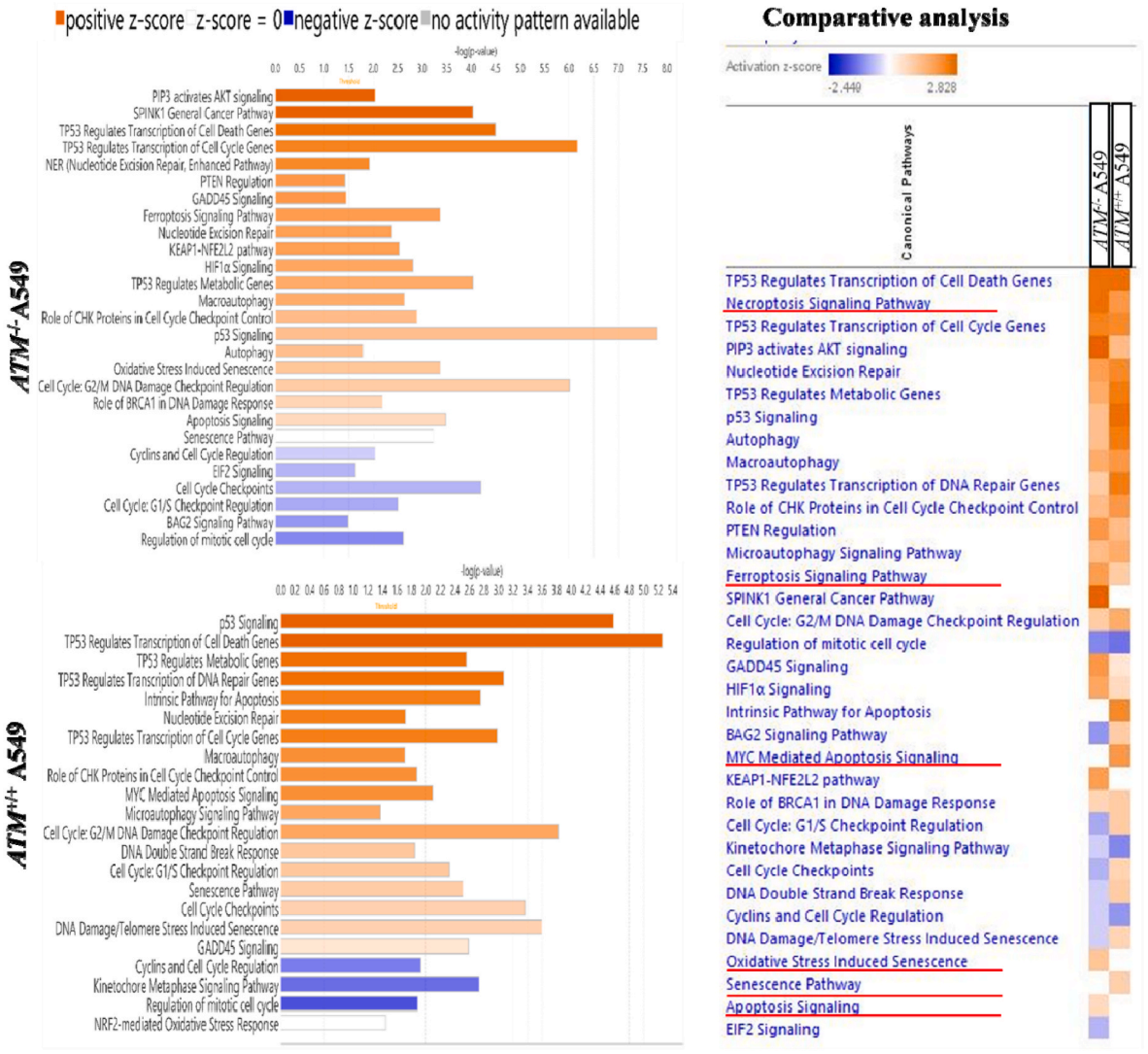

Fig. 5. Canonical pathway analysis of $ATM^{-/-}$ and $ATM^{+/+}$ A549 cells following cisplatin exposure. The figure includes a comparative analysis of the canonical pathways between the two groups.

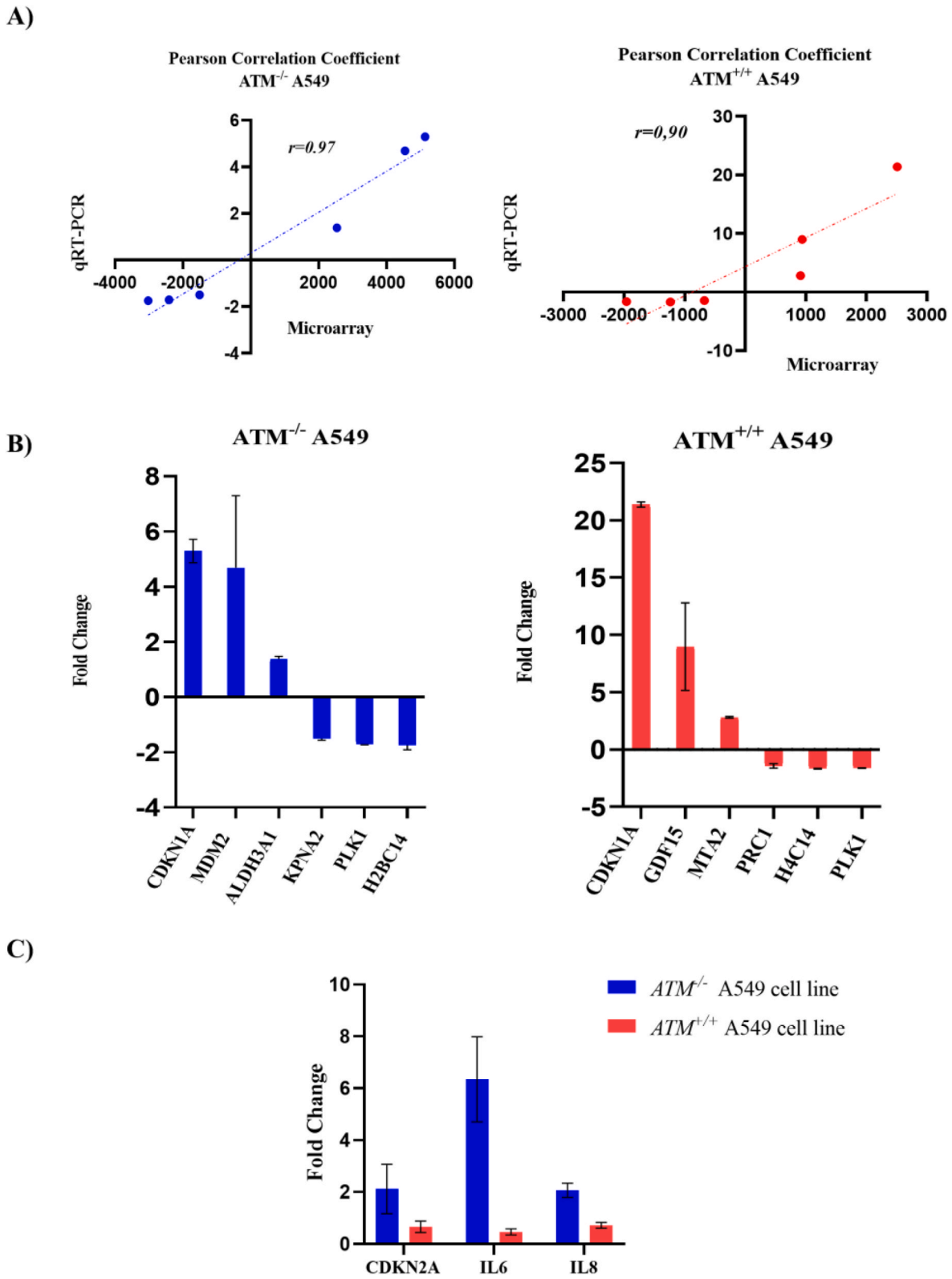

Fig. 6. A) Linear regressions and Pearson correlation coefficients for microarray and q-PCR data in $ATM^{-/-}$ A549 wild-type and $ATM^{+/+}$ A549 cells. **B)** Verification of the top three up and down-regulated genes by q-PCR in these cells. **C)** Significant upregulation of *CDKN2A, IL8* and *IL6* genes in $ATM^{-/-}$ A549 cancer cells, with the opposite trend in the A549 wild-type cells following cisplatin exposure.

3.10. Single cell electrophoresis (comet assay)

In order to assess DNA damage in $ATM^{+/+}$ A549 and $ATM^{-/-}$ A549 cells, we utilized the alkaline comet assay (as shown in Fig. 11). Especially, the alkaline comet assay is employed to assess oxidative DNA damage. Knockout of the *ATM* gene leads to a ROS increase, which exacerbated oxidative DNA damage, further supporting the tail formation observed in the comet assay. Moreover, the absence of *ATM*

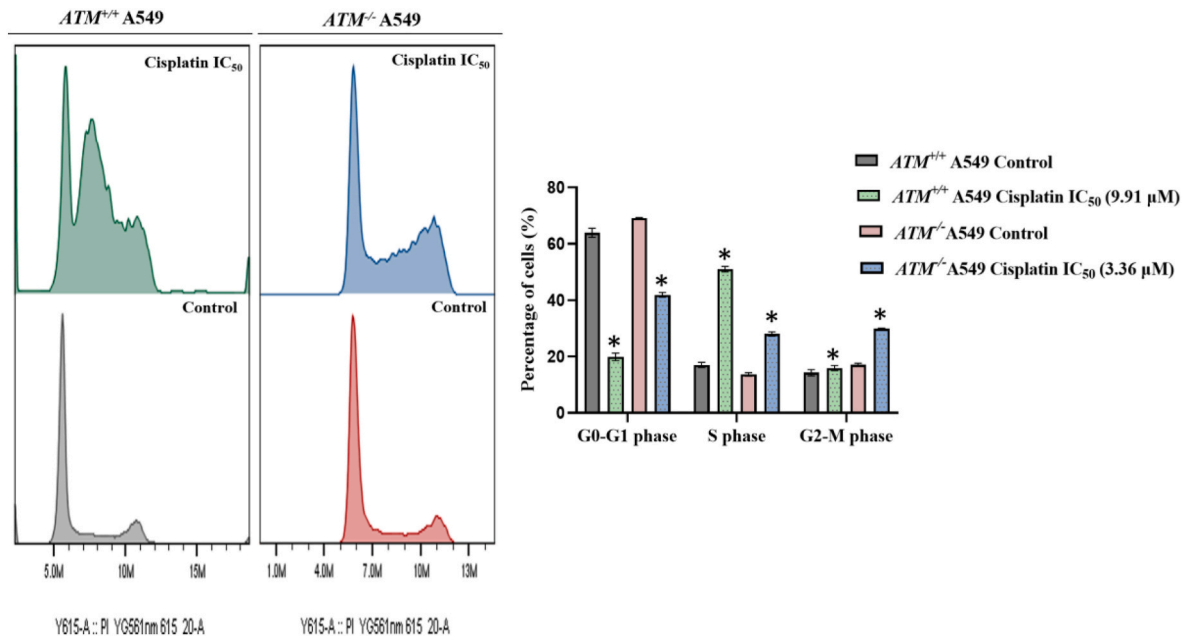

Fig. 7. Flow cytometric cell cycle analysis in $ATM^{+/+}$ and $ATM^{-/-}$ A549 cancer cell lines treated with the IC_{50} concentration of cisplatin. The statistical significance was analyzed using Student's t-test ($^*p < 0{,}05$).

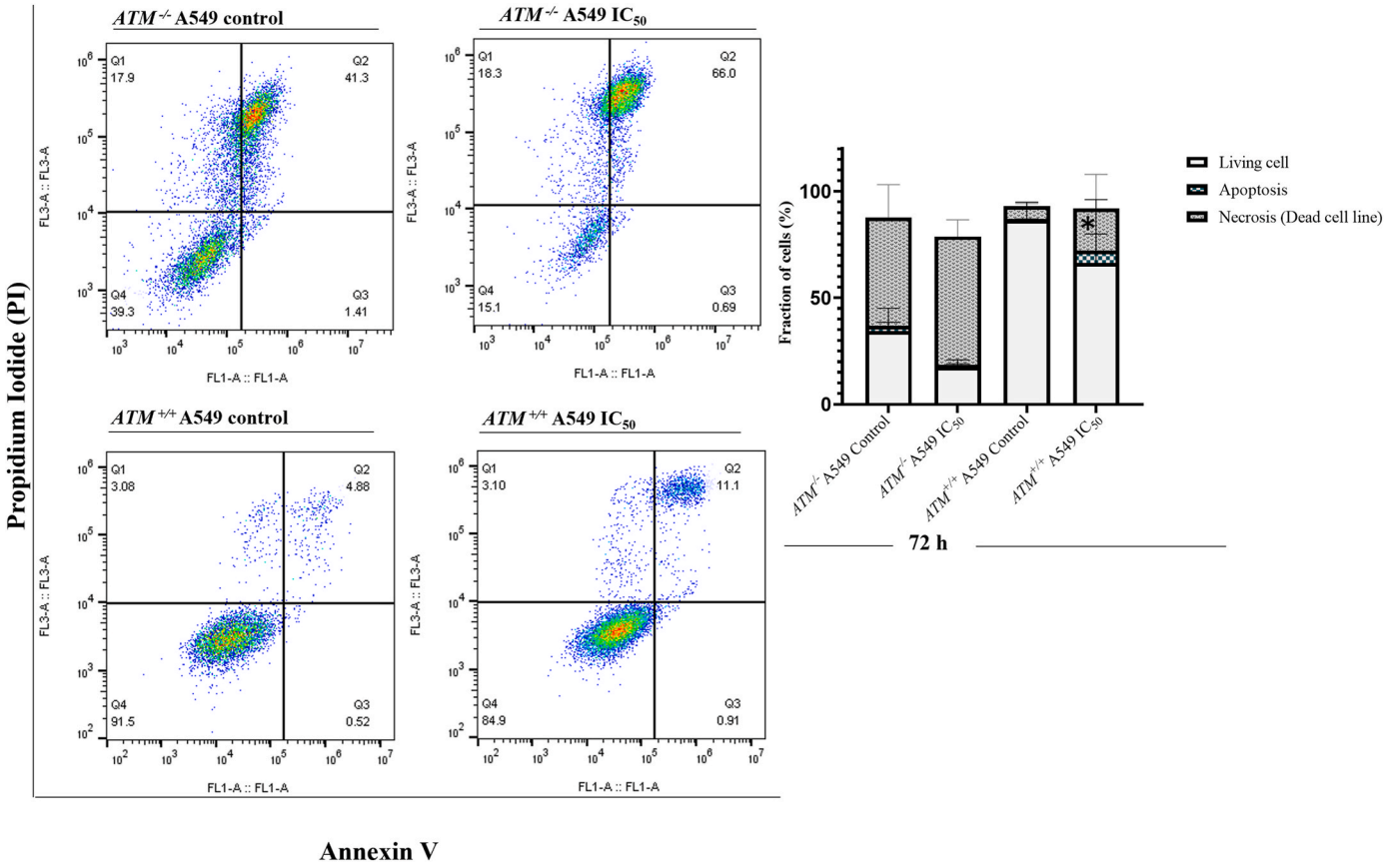

Fig. 8. Flow cytometric analysis for apoptosis in $ATM^{+/+}$ and $ATM^{-/-}$ A549 cancer cell lines treated with the IC_{50} concentration of cisplatin. The statistical significance was analyzed using Student's t-test ($^*p < 0{,}05$).

rendered cells more susceptible to the elevated ROS levels in the presence of cisplatin. The ATM knockout led to a significant increase in the tail moment of cells in the comet assay following cisplatin exposure. In contrast, we also observed a relatively lower comet tail moment in $ATM^{+/+}$ A549 cells. Cisplatin-induced DNA damage typically results in a reduced tail moment due to the formation of interstrand crosslinks. However, cisplatin not only causes DNA damage through the formation of interstrand crosslinks but also induces oxidative stress by increasing

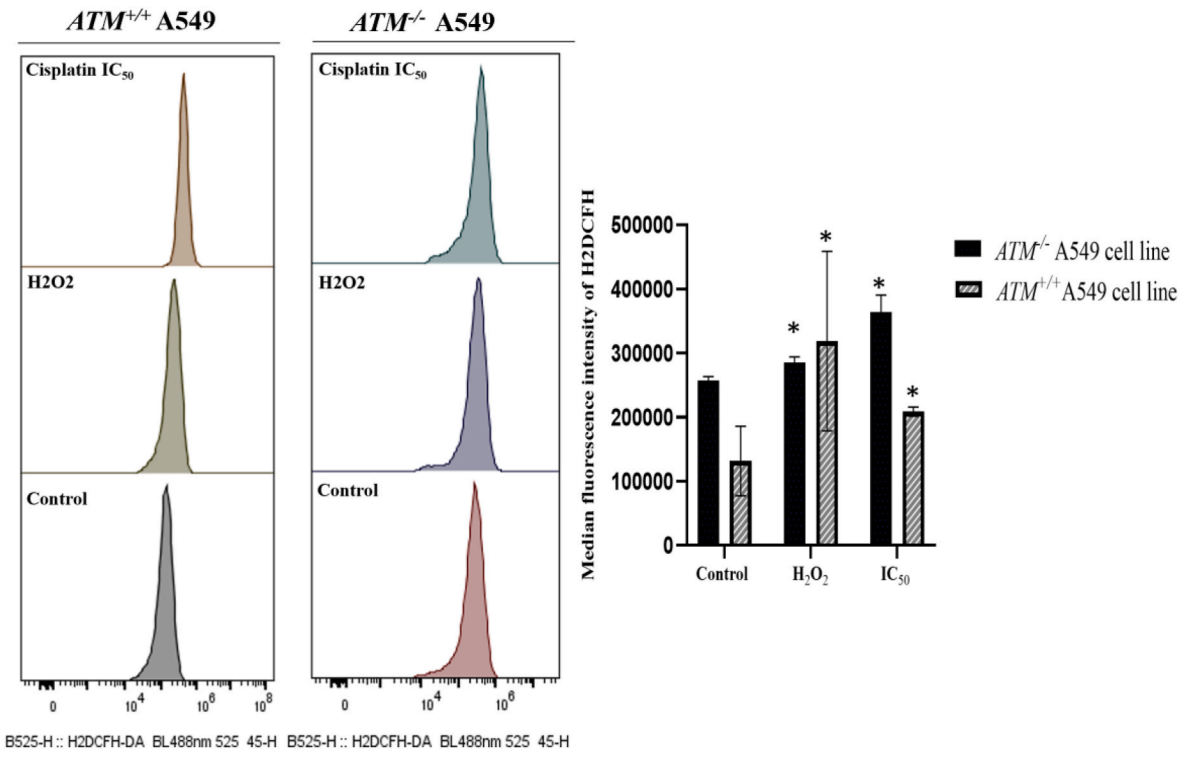

Fig. 9. Flow cytometric analysis to detect ROS levels in $ATM^{+/+}$ and $ATM^{-/-}$ A549 cancer cell lines treated with IC_{50} concentrations of cisplatin. The statistical significance was analyzed using Student's t-test ($*p < 0,05$).

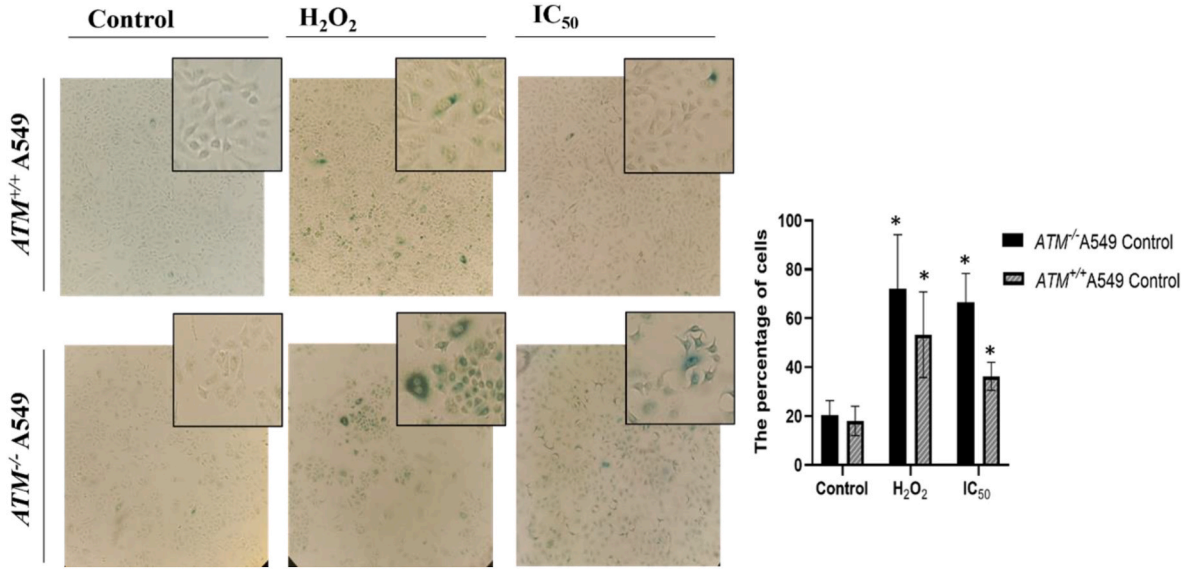

Fig. 10. Quantitative assessment of cellular senescence by staining senescence-associated β-galactosidase, following cisplatin exposure in $ATM^{+/+}$ and $ATM^{-/-}$ A549 cells.

ROS production, which may contribute to further DNA damage.

Our acquired data revealed a discernible disparity in the DNA damage profiles, with the $ATM^{-/-}$ A549 cell line manifesting heightened susceptibility to cisplatin-induced damage at a concentration of 3.36 μM. In comparison, the wild-type cell line exhibited a reduced percentage of DNA damage even upon exposure to a higher cisplatin concentration (9.91 μM). This observed discrepancy suggests that the absence of *ATM* renders cells considerably vulnerable to cisplatin.

4. Discussion

ATM, a key member of the phosphatidylinositol-3 kinase-related kinase (PIKK) family, plays a crucial role in the DNA damage response (DDR) by phosphorylating over 700 proteins, including p53, CHK2, and MDM2 [36–39]. These phosphorylations initiate signalling pathways such as apoptosis, senescence, and autophagy, maintaining cellular homeostasis [40]. However, arising mutations in *ATM* disrupt these mechanisms, contributing to aging, cancer progression, and therapy resistance.

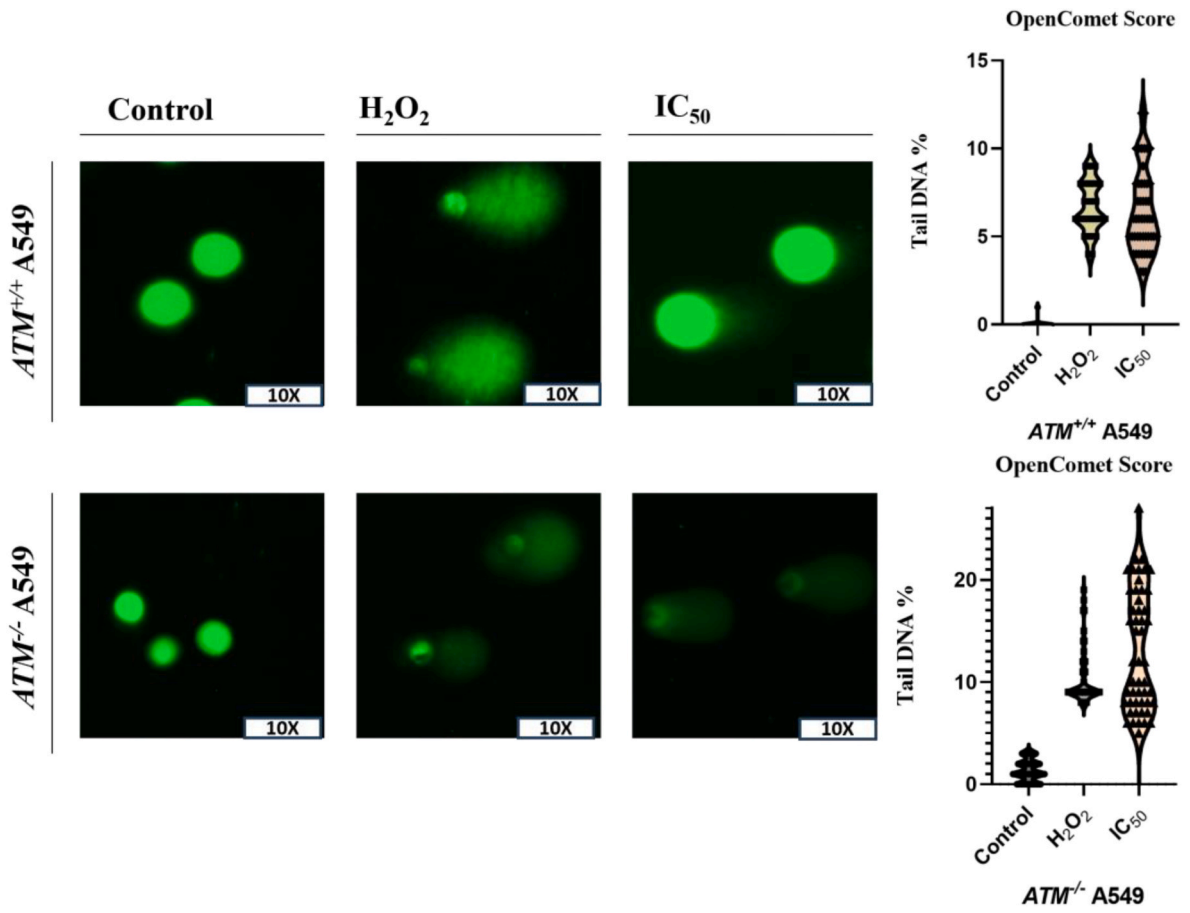

Fig. 11. Quantitative assessment of DNA damage using the alkaline comet assay, specifically single cell gel electrophoresis, following cisplatin exposure in $ATM^{+/+}$ and $ATM^{-/-}$ A549 cells. The 'tail DNA%' parameter was quantified based on the analysis of 50 randomly selected cells, as illustrated in the accompanying violin plot.

Whole-genome sequencing studies reveal that *ATM* mutations, particularly missense variants within the kinase domain, are prevalent in therapy-resistant cancers [39,41,42]. These mutations reduce ATM's kinase activity or protein expression, leading to impaired DDR and drug resistance [39,43]. However, the effect of mutations on drug resistance remains elusive. Hence, we performed a comparative analysis of multiple datasets in this study to select most predictive biomarkers in 23 cancer types. A comprehensive mutational analysis of 23 proteins involved in DSB mechanism was conducted across over 7500 tumors representing distinct cancer types in three parameters. The findings revealed that ATM exhibit the highest mutation frequency among the analyzed proteins. Particularly, missense mutations were observed to be the predominant type in ATM protein rather than frameshift and nonsense mutations. Mutation analysis executed via c-BioPortal reveals that the highest frequency of mutations in coding regions is observed in stomach, colorectal, bladder, breast, prostate, kidney, skin, head and neck, and lung cancer cases. These findings highlight the complex heterogeneity of various cancer cases, emphasizing the importance of tailoring treatment strategies based on cancer type. This underscores the necessity of developing personalized therapeutic approaches for effective cancer treatment management.

In addition, we conducted comprehensive bioinformatic analyses by using c-BioPortal to evaluate the effects of 23 proteins involved in the DSB mechanism across 23 different cancer types. From a broad perspective, our findings revealed that the high expression of identified biomarkers was associated with poor survival in liver, kidney, breast, and lung cancer cases according to various parameters (as shown in Supplementary Fig. 1). In the obtained data set, we observed that high expression of *ATM* was linked to poor survival exclusively in breast cancer. For lung cancer, the high expression of *RAD54B, XRCC6, XRCC3*, and *DCLRE1B* was identified as biomarkers associated with poor survival outcomes in distinct parameters (as shown in Fig. 2).

Platinum-based chemotherapies are cornerstone treatments for various cancers, exerting their cytotoxic effects primarily through DNA damage and the induction of apoptosis [44,45]. Prolonged use of platinum-based drug exposure increases mutation rates, altering drug responses and enabling cancer survival via alternative pathways. The most detrimental consequence of mutations is the limitation of cisplatin efficacy due to the development of resistance [46]. Combination therapies can delay resistance, but validating biomarkers as drug targets by experimental studies is necessary [47]. Therefore, we performed cytotoxic experiments to observe the consequences of *ATM* knockout in the presence of cisplatin. The results demonstrated that *ATM* knockout enhances cisplatin sensitivity. Considering the heterogeneity of mutations across different cancer types, experimental analyses tailored to specific cancer types are likely to provide greater opportunities for the development of personalized treatments.

Mechanistic insights from expression profiling data disclose the underlying mechanisms of increased cisplatin sensitivity. [48–52]. Senescence is a complex phenotype characterized by distinct changes in morphology, gene expression, metabolism, and other biological processes that occur in a time-dependent manner [53]. Cellular senescence is a fundamental stress response program that has evolved to serve specific physiological functions, including embryonic development and wound healing [54]. Currently, senescence is recognized as a highly dynamic state that is neither strictly irreversible nor fully reversible [54]. While *ATM* knockout has been previously shown to suppress senescence, our transcriptomic analysis reveals that ATM knockout

activates the oxidative damage induced senescence signalling pathway [48,55]. This activation occurs through an imbalance in cell death mechanisms caused by increased reactive oxygen species (ROS) levels.

In the presence of ATM, apoptosis is the predominant response to cisplatin treatment. However, *ATM* knockout shifts the balance, promoting necroptosis, ferroptosis, and oxidative damage-induced senescence. ATM acts as a defence mechanism, maintaining ROS levels within a manageable range [56]. If inhibited, ROS levels rise, triggering alternative cell death pathways to restore cellular homeostasis. Despite lower cisplatin concentrations, ROS accumulation was significantly higher in *ATM* knockout cells compared to wild-type A549 cancer cells, enhancing cisplatin sensitivity through oxidative damage-induced senescence.

To further investigate these mechanisms, we employed Ingenuity Pathway Analysis (IPA) and Chipster software to identify key genes involved. Our findings reveal a critical interplay between ATM and nuclear factor (erythroid-derived 2)-like 2 (NRF2). NRF2 is known as a central transcription regulator of the antioxidant response [57–59]. *NRF2* downregulation following *ATM* knockout reduces cellular resilience to oxidative stress, exacerbating ROS accumulation. Previously, *NRF2* inhibition suppressed the DNA damage response (DDR) by downregulating *ATM* and *ATR* expression, highlighting a critical feedback loop essential for maintaining cellular integrity [59]. However, there is no evidence of regulatory crosstalk between ATM and oxidative stress induced senescence through NRF2 downregulation.

The key point here is that prolonged cisplatin exposure, resulting in an increased mutation rate, may lead to changes in the drug's response. One of the potential reasons for resistance may be the inability of apoptotic signalling pathways to function as required in the presence of ATM. Existed mutations associated with ATM may hinder the cellular response to the administered drug. However, a potential solution to acquired resistance in cancer patients could be the activation of other cell death pathways through modified combination therapy strategies.

CRediT authorship contribution statement

Ayşegül Varol: Writing – review & editing, Writing – original draft, Methodology, Investigation, Data curation, Conceptualization. **Sabine M. Klauck:** Writing – review & editing, Software, Methodology, Investigation, Data curation, Conceptualization. **Susan P. Lees-Miller:** Methodology, Investigation. **Thomas Efferth:** Writing – review & editing, Supervision, Project administration, Conceptualization.

Declaration of competing interest

The authors declare the following financial interests/personal relationships which may be considered as potential competing interests: Aysegul Varol reports financial support was provided by Turkish Government (National Education Scholarship). If there are other authors, they declare that they have no known competing financial interests or personal relationships that could have appeared to influence the work reported in this paper.

Acknowledgement

We gratefully acknowledge the Microarray Unit of the Genomics and Proteomics Core Facility, German Cancer Research Center (DKFZ) Heidelberg, for providing excellent Expression Profiling service. We thank the Flow Cytometry Core Facility at the Institute of Molecular Biology (IMB, Mainz, Germany) for their kind training and technical support to complete the detection of reactive oxygen species and cell cycle experiments. A.V. is grateful for a stipend provided by the Turkish Government (National Education Scholarship).

Appendix A. Supplementary data

Supplementary data to this article can be found online at https://doi.org/10.1016/j.cbi.2025.111563.

Data availability

Data will be made available on request.

References

[1] B.N. Ames, Mutagenesis and carcinogenesis: endogenous and exogenous factors, Environ. Mol. Mutagen. 14 (S16) (1989) 66–77.
[2] R. De Bont, N. Van Larebeke, Endogenous DNA damage in humans: a review of quantitative data, Mutagenesis 19 (3) (2004) 169–185.
[3] A.M. Weber, A.J. Ryan, ATM and ATR as therapeutic targets in cancer, Pharmacol. Therapeut. 149 (2015) 124–138.
[4] N. Chatterjee, G.C. Walker, Mechanisms of DNA damage, repair, and mutagenesis, Environ. Mol. Mutagen. 58 (5) (2017) 235–263.
[5] A. Turchick, et al., Selective inhibition of ATM-dependent double-strand break repair and checkpoint control synergistically enhances the efficacy of ATR inhibitors, Mol. Cancer Therapeut. 22 (7) (2023) 859–872.
[6] X. Wu, et al., DNA damage response (DDR): a link between cellular senescence and human cytomegalovirus, Virol. J. 20 (1) (2023) 250.
[7] G.-M. Li, Mechanisms and functions of DNA mismatch repair, Cell Res. 18 (1) (2008) 85–98.
[8] C.D. McFarland, et al., Impact of deleterious passenger mutations on cancer progression, Proc. Natl. Acad. Sci. 110 (8) (2013) 2910–2915.
[9] C. Holohan, et al., Cancer drug resistance: an evolving paradigm, Nat. Rev. Cancer 13 (10) (2013) 714–726.
[10] A.-M. Florea, D. Büsselberg, Cisplatin as an anti-tumor drug: cellular mechanisms of activity, drug resistance and induced side effects, Cancers 3 (1) (2011) 1351–1371.
[11] A. Eastman, The mechanism of action of cisplatin: from adducts to apoptosis. Cisplatin: Chemistry and Biochemistry of a Leading Anticancer Drug, 1999, pp. 111–134.
[12] L.F. Qin, I.O. Ng, Induction of apoptosis by cisplatin and its effect on cell cycle-related proteins and cell cycle changes in hepatoma cells, Cancer Lett. 175 (1) (2002) 27–38.
[13] M. Kartalou, J.M. Essigmann, Mechanisms of resistance to cisplatin, Mutat. Res. Fund Mol. Mech. Mutagen 478 (1–2) (2001) 23–43.
[14] K. naidu gopal Hariprabu, M. Sathya, S. Vimalraj, CRISPR/Cas9 in cancer therapy: a review with a special focus on tumor angiogenesis, Int. J. Biol. Macromol. 192 (2021) 913–930.
[15] M. Vaghari-Tabari, et al., CRISPR/Cas9 gene editing: a new approach for overcoming drug resistance in cancer, Cell. Mol. Biol. Lett. 27 (1) (2022) 49.
[16] A.A. Aljabali, M. El-Tanani, M.M. Tambuwala, Principles of CRISPR-Cas9 technology: advancements in genome editing and emerging trends in drug delivery, J. Drug Deliv. Sci. Technol. (2024) 105338.
[17] A. Saber, et al., CRISPR/Cas9 for overcoming drug resistance in solid tumors, Daru 28 (2020) 295–304.
[18] D. Li, et al., Interactions between oxidative stress and senescence in cancer: mechanisms, therapeutic implications, and future perspectives, Redox Biol. 73 (2024) 103208.
[19] B. Li, et al., Distinct roles of c-Abl and Atm in oxidative stress response are mediated by protein kinase C δ, Gene Dev. 18 (15) (2004) 1824–1837.
[20] A. Agathanggelou, et al., Targeting the Ataxia Telangiectasia Mutated-null phenotype in chronic lymphocytic leukemia with pro-oxidants, Haematologica 100 (8) (2015) 1076.
[21] C. Yu, J.-H. Xiao, The Keap1-Nrf2 system: a mediator between oxidative stress and aging, Oxid. Med. Cell. Longev. 2021 (1) (2021) 6635460.
[22] E. Cerami, et al., The cBio cancer genomics portal: an open platform for exploring multidimensional cancer genomics data, Cancer Discov. 2 (5) (2012) 401–404.
[23] J. Gao, et al., Integrative analysis of complex cancer genomics and clinical profiles using the cBioPortal, Sci. Signal. 6 (269) (2013) pl1-pl1.
[24] B. Győrffy, Integrated analysis of public datasets for the discovery and validation of survival-associated genes in solid tumors, Innovation 5 (3) (2024).
[25] A. Varol, et al., Enhancing cisplatin drug sensitivity through PARP3 inhibition: the influence on PDGF and G-coupled signal pathways in cancer, Chem. Biol. Interact. (2024) 111094.
[26] N.R. Jette, et al., Combined poly-ADP ribose polymerase and ataxia-telangiectasia mutated/Rad3-related inhibition targets ataxia-telangiectasia mutated-deficient lung cancer cells, Br. J. Cancer 121 (7) (2019) 600–610.
[27] J. O'brien, et al., Investigation of the Alamar Blue (resazurin) fluorescent dye for the assessment of mammalian cell cytotoxicity, Eur. J. Biochem. 267 (17) (2000) 5421–5426.
[28] J. Petiti, L. Revel, C. Divieto, Standard operating procedure to optimize resazurin-based viability assays, Biosensors 14 (4) (2024) 156.
[29] K.J. Livak, T.D. Schmittgen, Analysis of relative gene expression data using real-time quantitative PCR and the 2− ΔΔCT method, Methods 25 (4) (2001) 402–408.
[30] I. Vermes, et al., A novel assay for apoptosis flow cytometric detection of phosphatidylserine expression on early apoptotic cells using fluorescein labelled annexin V, J. Immunol. Methods 184 (1) (1995) 39–51.
[31] M.E. Saeed, et al., Disruption of lipid raft microdomains, regulation of cd38, tp53, and myc signaling, and induction of apoptosis by lomitapide in multiple myeloma cells, Cancer Genom. Proteom. 19 (5) (2022) 540–555.

[32] N.N. Hooten, M.K. Evans, Techniques to induce and quantify cellular senescence, J. Vis. Exp. 123 (2017).
[33] B.M. Gyori, et al., OpenComet: an automated tool for comet assay image analysis, Redox Biol. 2 (2014) 457–465.
[34] P. Ortiz-Montero, A. Londoño-Vallejo, J.-P. Vernot, Senescence-associated IL-6 and IL-8 cytokines induce a self-and cross-reinforced senescence/inflammatory milieu strengthening tumorigenic capabilities in the MCF-7 breast cancer cell line, Cell Commun. Signal. 15 (2017) 1–18.
[35] C.A. Schmitt, B. Wang, M. Demaria, Senescence and cancer—role and therapeutic opportunities, Nat. Rev. Clin. Oncol. 19 (10) (2022) 619–636.
[36] N.R. Jette, et al., ATM-deficient cancers provide new opportunities for precision oncology, Cancers 12 (3) (2020) 687.
[37] S. Matsuoka, et al., ATM and ATR substrate analysis reveals extensive protein networks responsive to DNA damage, Science 316 (5828) (2007) 1160–1166.
[38] D. Menolfi, S. Zha, ATM, ATR and DNA-PKcs kinases—the lessons from the mouse models: inhibition≠ deletion, Cell Biosci. 10 (1) (2020) 8.
[39] S. Putti, et al., ATM kinase dead: from ataxia telangiectasia syndrome to cancer, Cancers 13 (21) (2021) 5498.
[40] V. Stagni, et al., ATM kinase-dependent regulation of autophagy: a key player in senescence? Front. Cell Dev. Biol. 8 (2021) 599048.
[41] M. Choi, T. Kipps, R. Kurzrock, ATM mutations in cancer: therapeutic implications, Mol. Cancer Therapeut. 15 (8) (2016) 1781–1791.
[42] K. Yamamoto, et al., Kinase-dead ATM protein is highly oncogenic and can be preferentially targeted by Topo-isomerase I inhibitors, eLife 5 (2016) e14709.
[43] Y. Zhou, et al., ATM deficiency confers specific therapeutic vulnerabilities in bladder cancer, Sci. Adv. 9 (47) (2023) eadg2263.
[44] E. Stefàno, et al., An overview of altered pathways associated with sensitivity to platinum-based chemotherapy in neuroendocrine tumors: strengths and prospects, Int. J. Mol. Sci. 25 (16) (2024) 8568.
[45] T. Boulikas, M. Vougiouka, Cisplatin and platinum drugs at the molecular level, Oncol. Rep. 10 (6) (2003) 1663–1682.
[46] D.J. Stewart, Mechanisms of resistance to cisplatin and carboplatin, Crit. Rev. Oncol.-Hematol. 63 (1) (2007) 12–31.
[47] L. Wang, L. Lankhorst, R. Bernards, Exploiting senescence for the treatment of cancer, Nat. Rev. Cancer 22 (6) (2022) 340–355.
[48] K.M. Aird, R. Zhang, ATM in senescence, Oncotarget 6 (17) (2015) 14729.
[49] J. Campisi, F. d'Adda di Fagagna, Cellular senescence: when bad things happen to good cells, Nat. Rev. Mol. Cell Biol. 8 (9) (2007) 729–740.
[50] H.T. Kang, et al., Chemical screening identifies ATM as a target for alleviating senescence, Nat. Chem. Biol. 13 (6) (2017) 616–623.
[51] J. Zhao, et al., ATM is a key driver of NF-κB-dependent DNA-damage-induced senescence, stem cell dysfunction and aging, Aging (Albany NY) 12 (6) (2020) 4688.
[52] J.M. Van Deursen, The role of senescent cells in ageing, Nature 509 (7501) (2014) 439–446.
[53] M. Eppard, J.F. Passos, S. Victorelli, Telomeres, cellular senescence, and aging: past and future, Biogerontology 25 (2) (2024) 329–339.
[54] M. Reimann, S. Lee, C.A. Schmitt, Cellular senescence: neither irreversible nor reversible, J. Exp. Med. 221 (4) (2024) e20232136.
[55] M.U. Kuk, et al., Alleviation of senescence via ATM inhibition in accelerated aging models, Mol. Cells 42 (3) (2019) 210–217.
[56] J.-H. Lee, Oxidative stress and the multifaceted roles of ATM in maintaining cellular redox homeostasis, Redox Biol. 75 (2024) 103269.
[57] S.K. Niture, R. Khatri, A.K. Jaiswal, Regulation of Nrf2—an update, Free Radic. Biol. Med. 66 (2014) 36–44.
[58] W. Li, A.N. Kong, Molecular mechanisms of Nrf2-mediated antioxidant response, Mol. Carcinog.: Publ. Cooperat. University of Texas MD Anderson Cancer Center 48 (2) (2009) 91–104.
[59] H.S. Khalil, Y. Deeni, NRF2 inhibition causes repression of ATM and ATR expression leading to aberrant DNA Damage Response, BioDiscovery 15 (2015) e8964.